

crack growth analyses were performed for the case of residual stress only and for residual stress with service loading. The crack growth portions of these analyses are discussed in Section G.7.

The finite element model used for the analyses is shown in Figure G.24. Note that the entire long length of pipe from the nozzle to the steam generator is included. It was originally thought that the long length of pipe could have an effect on the predicted weld residual stresses. However, two analyses were performed here: one with a free end (in the Type 304 stainless steel length of pipe), and one with the length of pipe extending to the steam generator. It turns out that the weld residual stresses are not affected much by the length of the pipe. However, for the thermal loading (discussed next), it was important to include this length of pipe to accurately predict service axial stresses.

Figure G.25 shows sequence plots of axial and hoop residual stresses after buttering and after post weld heat treatment. It is clearly seen that residual stresses are strongly affected by the PWHT. The hoop stresses are relaxed quite significantly. Figure G.26 illustrates the equivalent plastic strains after buttering and after PWHT. After PWHT, plastic strains do increase somewhat more compared with the similar cold leg results (Figure G.10). Corresponding creep strains after PWHT are illustrated in Figure G.27. It is these creep strains that relax the weld induced residual stresses.

G.6.3 Hot Leg Computational Weld Model Results

Figure G.28 (a) and (b) shows axial and hoop stresses after depositing the first 18 mm (0.7 inch) of weld on the inside of the pipe and after depositing the bridge layer. The bridge layer was apparently deposited to keep the pipes together during grinding and re-deposition of new weld passes. It is interesting to note that, due to global bending, compressive axial stresses (Figure G.28 (a)) develop before removal of the material. Figure G.28 (c) and (d) show the maximum and minimum principle

stresses after removal of the weld metal with only the bridge material remaining.

Figure G.29 shows axial and hoop residual stresses before repair (i.e., before grinding and re-deposition of weld metal) and after depositing the repair weld (inside weld repair case). Axial stresses actually reverse sign after the repair and the hoop stresses increase in magnitude after the inside repair.

Figure G.30 shows axial residual stresses after the repair is complete. Two cases are shown: one where the inside weld is deposited first following repair, followed by the outer passes, and vice-versa. As discussed above, both cases are considered since the complete repair sequence is not known. The outline of the buttering layer and the weld material is shown for convenience. *It is important to note that axial residual stresses are more tensile, and cover a larger area at the inner surface of the pipe for the outside deposition first followed by inside welding.* This suggests that circumferential PWSCC (caused by axial stresses) is more likely for the outside weld first case. These results, and the model itself, can be used to define optimum weld sequencing for both repairs and for original welding. Figure G.31 shows a similar comparison for hoop residual stresses for the two sequences. Again, the outside weld repair first case produces larger hoop residual stresses along the inner pipe surface compared with the inside weld first case. Axial cracking is expected to be more severe for this case as well. This will be further shown in Section G.7, which discusses PWSCC analyses.

Figures G.32 through G.35 provide comparisons of residual plastic strains caused by welding between the two sequences. In all cases except for shear strains (Figure G.35), residual plastic strains are larger in magnitude, and cover a larger area for the outside weld first case.

Figure G.36 shows the axial residual stress state after applying a hydro-test pressure at room temperature to the pipe over top the weld induced residual stresses. Hydro-test analysis assumes an end cap condition so axial stresses

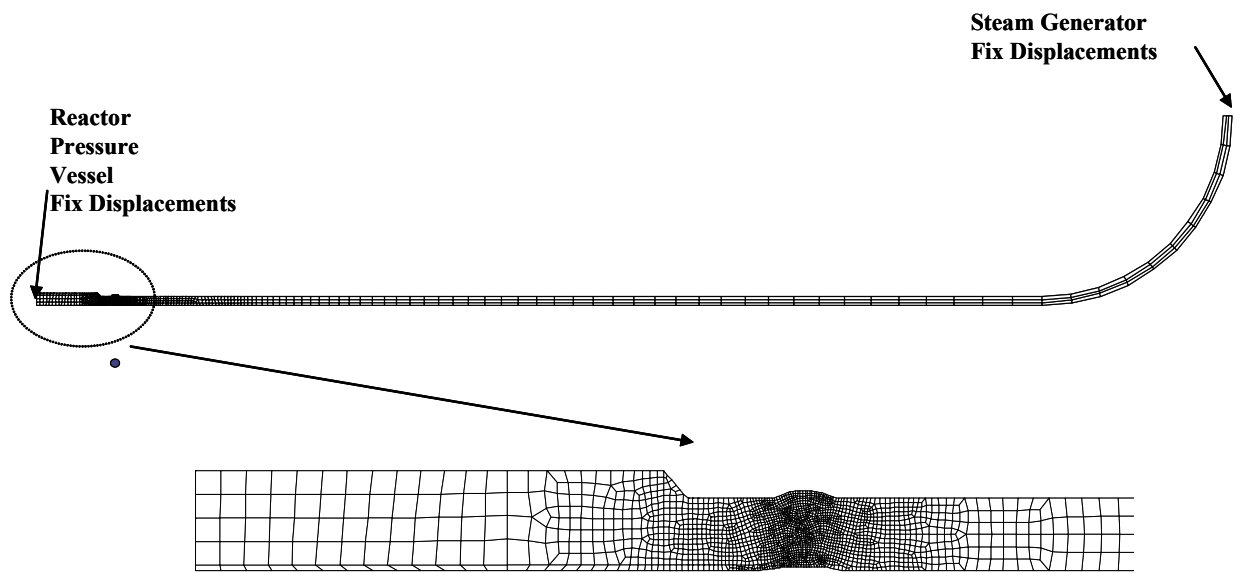


Figure G.24 Full finite element model

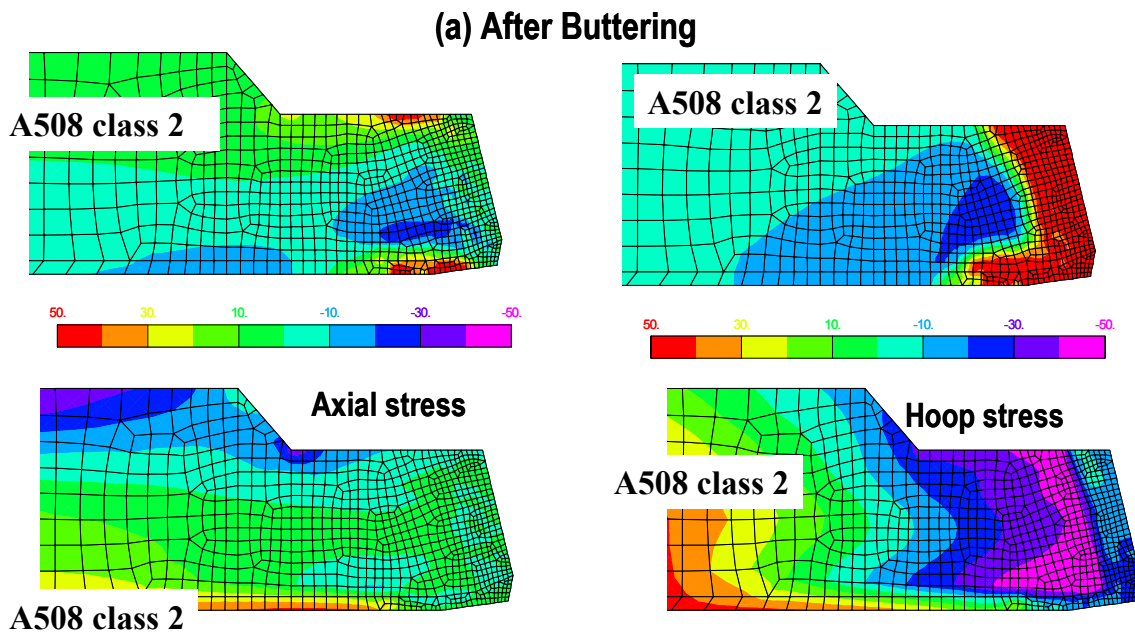
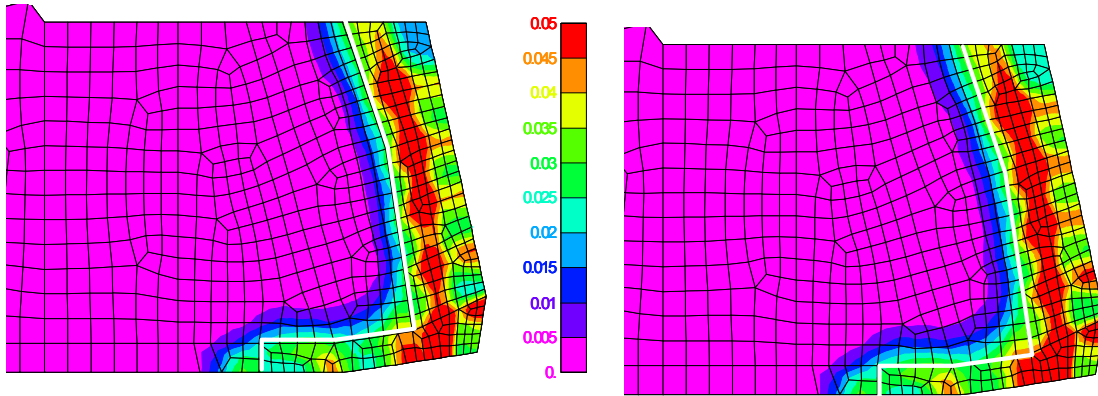


Figure G.25 Cladding simulation stresses (after cooling to room temperature)



(a) End of Cladding

(b) End of Post cladding heat treatment

Figure G.26 Cladding simulation – effective plastic strains

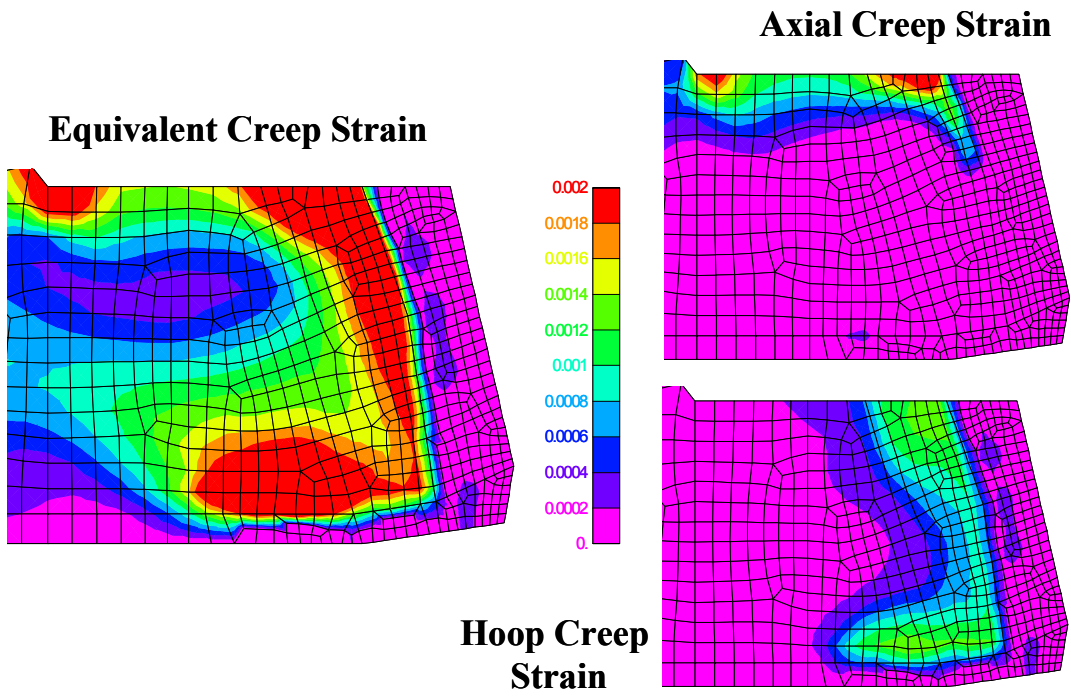


Figure G.27 Post cladding heat treatment simulation – creep strains

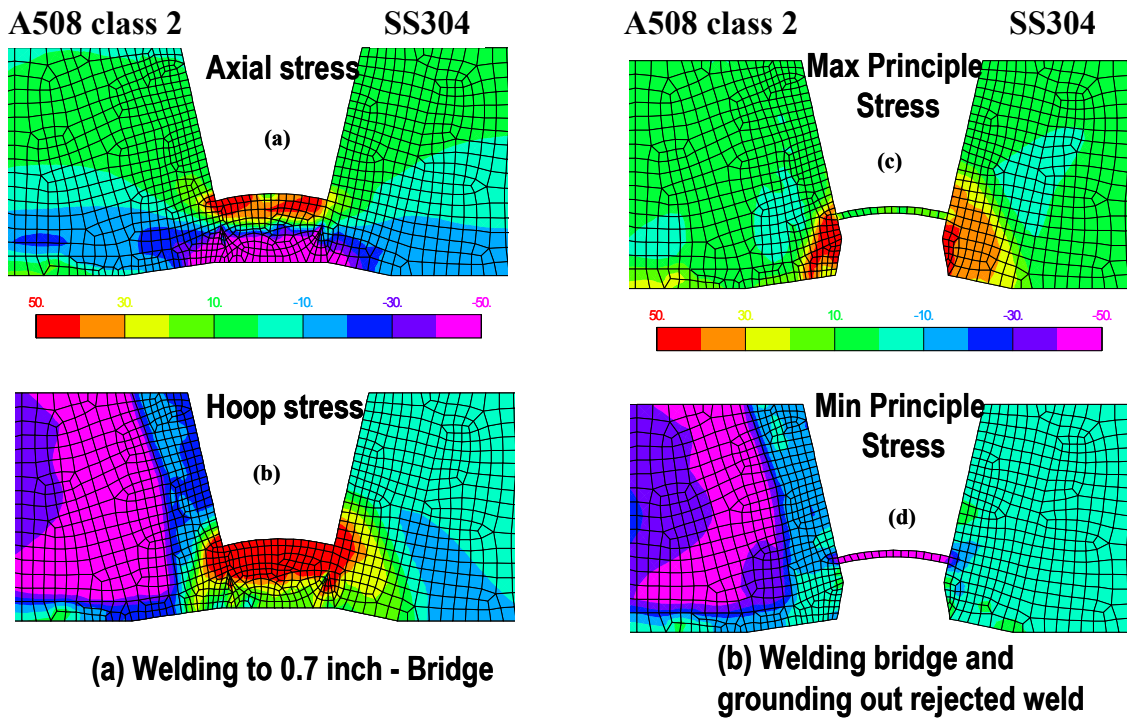


Figure G.28 Rejected weld and bridge simulation

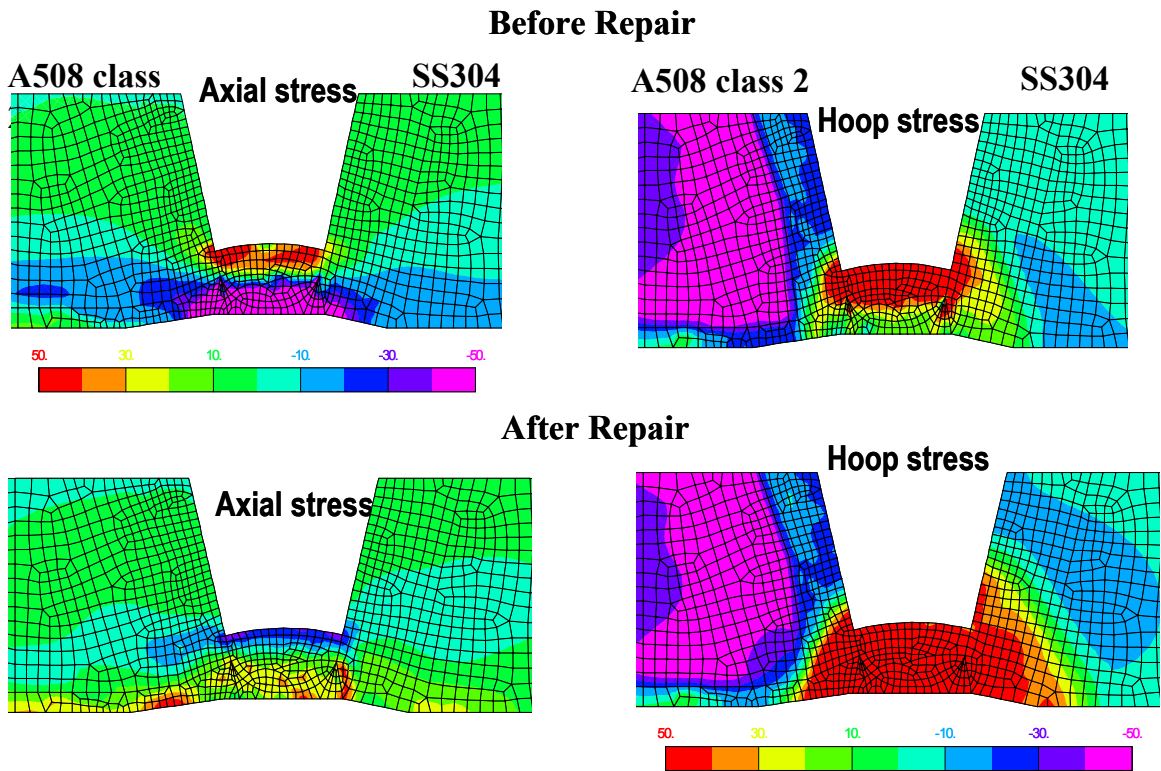


Figure G.29 Comparison of rejected weld and bridge simulation